A Finite Element Multifield Model for Critical Loads of Composite Laminated Plates

Riccardo Battaglia[1], Antonio Tralli[1], Antonio Cazzani[2]
[1]*Department of Engineering (DI), University of Ferrara, Italy*
E-mail: riccardo.battaglia@unife.it, tra@unife.it

[2]*Department of Structural, Infrastructural and Geomatics Engineering (DISIG), University of Cagliari, Italy*
E-mail: antonio.cazzani@unica.it

Keywords: Laminated composite plates, critical loads, hybrid finite elements, shear-locking.

SUMMARY. Fibre-reinforced plates and shells are finding an increasing interest in engineering applications, because they are light-weight and provide a high stiffness over weight ratio. Consequently, efficient and robust computational tools are required for the analysis of such structural models. It should be remarked that because of their slenderness these structural elements require a careful evaluation of their safety with reference to buckling phenomena.

1 INTRODUCTION

A huge amount of laminated finite elements have been developed and incorporated in most commercial codes for structural analysis: a partial survey can be found in [1]. In this paper, as a sequel of some previous works already published by the Authors [2], [3], an assumed-strain laminated plate element is derived within the framework of the First-order Shear Deformation Theory (i.e., by assuming that particles of the plate originally lying along a straight line which is normal to the undeformed middle surface remain aligned along a straight line during the deformation process), along with the hypothesis of perfect bonding between laminae. The *in-plane* components of the (infinitesimal) strain tensor are interpolated and, by making use of the constitutive law, the corresponding in-plane stress distribution is deduced for each layer. *Out-of-plane* shear stresses are then computed by integrating the equilibrium equations in each lamina, account taken of their continuity requirements. The corresponding out-of-plane shear strains are finally obtained via inverse constitutive law. The resulting global strain field depends on a fixed number of parameters, regardless of the total number of layers: 12 degrees of freedom are assumed, for instance, in the rectangular element which has been developed. The model does not suffer shear-locking phenomena even in the thin plate limit and provides an accurate description of interlaminar stresses. In this new mixed-hybrid element the nodal variables are, as usual, the vertical displacement and the two rotations about the in-plane axes; both cases of Lagrangian and Hermitian polynomial interpolation have been investigated. While the former choice is effective even in the thick limit, the latter choice (which enforces displacement and rotations continuity at the interelement boundaries, whereas the normal derivatives of the displacement field are allowed to be discontinuous) seems to be more appropriate for thin plates. In dealing with stability analysis, second-order strain components are deduced from the displacement field and the Green-Lagrange strain tensor is employed; it should be emphasized that in the thin-limit case (i.e. in the case when Love-Kirchhoff theory applies) the standard geometric stiffness matrix, associated to the same displacement field, is recovered. Moreover the presented model allows to evaluate accurately the influence of shear deformations on critical loads: such an effect is expected to be significant in typical technical applications of composite laminated plates.

From a computational point of view the performances of the developed element appear fair when compared in terms of efficiency and accuracy with other elements proposed in the technical literature and/or implemented in available commercial finite element codes.

2 THE MODEL

A laminated plate is here considered: a thin/moderately thick flat body, composed by K layers with different mechanical characteristics, stacked one above the other and occupying the domain:

$$\Omega \;=\; \left\{(x_1, x_2, x_3) \in R^3 \mid x_3 \in [-h/2, +h/2],\ (x_1, x_2) \in \tilde{\Omega} \subset R^2\right\}. \tag{1}$$

Plane $\tilde{\Omega}$ (i.e. $x_3 = 0$) defines the middle surface of the undeformed plate, as it is shown in Figure 1.

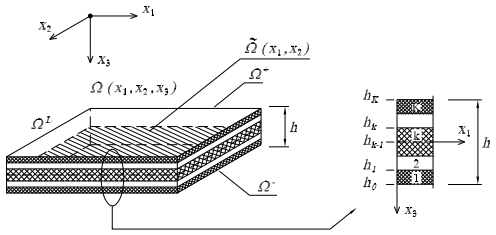

Figure 1: A typical laminated plate.

For the sake of simplicity, only laminates in the framework of linear elasticity will be considered, but in view of application to buckling problems stretching effects will be explicitly taken into account.

Layers lie parallel to the middle surface $\tilde{\Omega}$; the typical k-th layer is bounded by thickness coordinates h_{k-1} and h_k and is supposed to be orthotropic with material axes oriented at an angle θ^k with reference to the laminate coordinate x_1. As a consequence, its elastic behaviour is completely defined by these 6 independent coefficients, written in the compact Voigt notation: C^k_{11}, C^k_{12}, C^k_{22}, C^k_{66}, C^k_{44} and C^k_{55}.

2.1 *Strain and stress fields*

Perfect bonding between laminae is assumed, so that *in-plane* strain components of the plate ε_{11}, ε_{22}, $\varepsilon_{12} = \varepsilon_{12}$ are given by the following global description:

$$\varepsilon_{11}(x_1, x_2, x_3) \;=\; \varepsilon^0_{11}(x_1, x_2) + x_3\tilde{\varepsilon}_{11}(x_1, x_2) \tag{2}$$

$$\varepsilon_{22}(x_1, x_2, x_3) \;=\; \varepsilon^0_{22}(x_1, x_2) + x_3\tilde{\varepsilon}_{22}(x_1, x_2) \tag{3}$$

$$\varepsilon_{12}(x_1, x_2, x_3) \;=\; \varepsilon^0_{12}(x_1, x_2) + x_3\tilde{\varepsilon}_{12}(x_1, x_2). \tag{4}$$

According to Eq. (2)–(4) the *in-plane* components of the infinitesimal strain tensor ε_{ij} consist of a stretching contribution, ε^0_{ij}, and of one, $x_3\tilde{\varepsilon}_{ij}$, which is linearly varying along the thickness, as in the classical plate theory.

By making use of the Constitutive Law (CL) enforced at the local level for the k-th lamina, these *in-plane* stress components (σ^k_{11}, σ^k_{22}, $\sigma^k_{12} = \sigma^k_{21}$) result:

$$\sigma^k_{11}(x_1, x_2, x_3) \;=\; C^k_{11}[\varepsilon^0_{11}(x_1, x_2) + x_3\tilde{\varepsilon}_{11}(x_1, x_2)] + C^k_{12}[\varepsilon^0_{22}(x_1, x_2) + x_3\tilde{\varepsilon}_{22}(x_1, x_2)] \tag{5}$$

$$\sigma^k_{22}(x_1, x_2, x_3) \;=\; C^k_{12}[\varepsilon^0_{11}(x_1, x_2) + x_3\tilde{\varepsilon}_{11}(x_1, x_2)] + C^k_{22}[\varepsilon^0_{22}(x_1, x_2) + x_3\tilde{\varepsilon}_{22}(x_1, x_2)] \tag{6}$$

$$\sigma^k_{12}(x_1, x_2, x_3) \;=\; 2C^k_{66}[\varepsilon^0_{12}(x_1, x_2) + x_3\tilde{\varepsilon}_{12}(x_1, x_2)]. \tag{7}$$

In general, these components, which vary linearly along the transverse direction of the lamina, are discontinuous at the interface between two laminae having different orientation and/or material properties.

When labels of the stress components are chosen in such a way that the former denotes the direction, and the latter the normal to the face they refer to, in absence of body forces the Linear Momentum Balance (LMB) equations for the k-th layer in the x_1 and x_2 directions read:

$$\sigma^k_{13,3} = -(\sigma^k_{11,1} + \sigma^k_{12,2}) \tag{8}$$

$$\sigma^k_{23,3} = -(\sigma^k_{21,1} + \sigma^k_{22,2}). \tag{9}$$

By integrating with respect to x_3 eqs. (8)–(9) the *out-of plane* components of the stress field in the k-th layer, $\sigma^k_{31} = \sigma^k_{13}$, $\sigma^k_{32} = \sigma^k_{23}$ can be derived explicitly, and the integrating constants can be defined in such a way that Traction Boundary Conditions (TBC) can be exactly fulfilled on the plate bases Ω^+ and Ω^-.

Once the transverse shear stresses are known, by making use of the inverse CL the corresponding *out-of-plane* shear strain components can be evaluated for the k-th lamina:

$$\varepsilon^k_{13} = \frac{\sigma^k_{13}}{2C^k_{55}} \qquad\qquad \varepsilon^k_{23} = \frac{\sigma^k_{23}}{2C^k_{44}}. \tag{10}$$

2.2 *Displacement field*

The kinematics of the laminated plate can be written in this way:

$$u_1(x_1, x_2, x_3) = u^0_1(x_1, x_2) - x_3\tilde{\varphi}_1(x_1, x_2) \tag{11}$$

$$u_2(x_1, x_2, x_3) = u^0_2(x_1, x_2) - x_3\tilde{\varphi}_2(x_1, x_2) \tag{12}$$

$$u_3(x_1, x_2, x_3) = \tilde{u}_3(x_1, x_2). \tag{13}$$

The *in-plane* components of the displacement field, u_j (with $j = 1, 2$), given by eqs. (11)–(12) consist of an extensional contribution, u^0_j and a flexural one, $x_3\tilde{\varphi}_j$, which is assumed, analogously to the classical Reissner-Mindlin model, to vary linearly along the transverse direction of the laminated plate; here $\tilde{\varphi}_j$ are the rotations (see Figure 2) of the transverse line elements, which initially lie perpendicular to the middle surface, about the x_j-axis. The normal component, expressed by (13), is instead assumed to be constant along the x_3-axis.

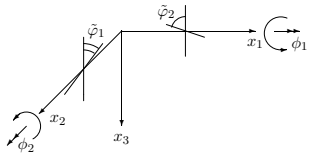

Figure 2: Rotations of the transverse line element of the plate $\tilde{\varphi}_1$ and $\tilde{\varphi}_2$.

2.3 *Variational formulation*

A brief deduction of an assumed-strain hybrid finite element is presented. A 3-D continuum is considered, occupying a volume Ω, bounded by a smooth surface $\partial\Omega = \partial\Omega_u \cup \partial\Omega_s$, with $\partial\Omega_u \cap$

$\partial\Omega_s = \emptyset$; $\partial\Omega_u$ is the portion of the boundary where the displacement field is prescribed, whereas $\partial\Omega_s$ is the complementary part of the boundary, where TBCs must be fulfilled.

To deal with the the buckling load problem, the following three-field variational principle (corresponding to a generalized form of the Hu-Washizu functional, see [4], [5]) can be stated:

$$\begin{aligned}\Pi_{HW}(\sigma_{ij},\varepsilon_{ij},u_i) &= \int_\Omega (\frac{1}{2}C_{ijmn}\varepsilon_{ij}\varepsilon_{mn} - b_i u_i)\mathrm{d}V \\ &- \int_\Omega \sigma_{ij}[\varepsilon_{ij} - \frac{1}{2}(u_{i,j}+u_{j,i})]\mathrm{d}V + \int_\Omega \frac{1}{2}\sigma^0_{ij}u_{l,i}u_{l,j}\mathrm{d}V \\ &- \int_{\partial\Omega_s} f_i u_i \mathrm{d}S - \int_{\partial\Omega_u} \sigma_{ij}n_j(u_i-\bar{u}_i)\mathrm{d}S. \end{aligned} \tag{14}$$

In eq. (14) $C_{ijmn}, \sigma_{ij}, \varepsilon_{ij}, u_i$ denote, respectively, the Cartesian components of the elasticity tensor, of stress and strain tensors and of the displacement vector; b_i and f_i denote the components of body and surface forces respectively, while $\bar{u}_i$ are the prescribed displacement components. σ^0_{ij} represents the (known) stress tensor in the *pre-critical* state, and the corresponding term provides the second-order work contribution.

If CL is *a priori* enforced, then it is possible to eliminate the stress components from Eq. (14), obtaining this *modified* Hu-Washizu functional, depending only on strain and displacement fields:

$$\begin{aligned}\Pi_{HW,mod}(\varepsilon_{ij},u_i) &= -\frac{1}{2}\int_\Omega C_{ijmn}\varepsilon_{ij}\varepsilon_{mn}\mathrm{d}V \\ &+ \int_\Omega (C_{ijmn}\varepsilon_{mn,j} - b_i)u_i\mathrm{d}V + \int_\Omega \frac{1}{2}\sigma^0_{ij}u_{l,i}u_{l,j}\mathrm{d}V \\ &+ \text{boundary terms.}\end{aligned} \tag{15}$$

If, instead of a continuous homogeneous solid, a laminated body is considered, which satisfies the previously introduced hypotheses, the variational principle must be modified accordingly. For a hybrid type laminate element, in the absence of body forces, the discretized version of functional (15) is:

$$\begin{aligned}\Pi^{H,e}_{HW,mod}(\varepsilon_{ij},u_i,\hat{u}_i) = -\sum_{k=1}^{K}\Bigg[&\frac{1}{2}\int_{\tilde{\Omega}^e}\int_{h_{k-1}}^{h_k} C^k_{ijmn}\varepsilon^k_{ij}\varepsilon^k_{mn}\mathrm{d}x_3\mathrm{d}A \\ &+ \int_{\tilde{\Omega}^e}\int_{h_{k-1}}^{h_k} C^k_{ijmn}\varepsilon^k_{mn,j}u_i\mathrm{d}x_3\mathrm{d}A + \frac{1}{2}\int_{\tilde{\Omega}^e}\int_{h_{k-1}}^{h_k}\sigma^{0k}_{ij}u_{l,i}u_{l,j}\mathrm{d}x_3\mathrm{d}A \\ &+ \int_{\Omega^{Le}}\int_{h_{k-1}}^{h_k} C^k_{ijmn}\varepsilon^k_{mn}n_j\hat{u}_i\mathrm{d}x_3\mathrm{d}l\Bigg],\end{aligned} \tag{16}$$

where $\hat{u}_i$ is a displacement field defined only on the boundary Ω^{Le} of the e-th element, whose domain is $\tilde{\Omega}^e$.

2.4 *Discretization of the strain and displacement field*

For a rectangular laminated plate element, the *in-plane* stretching contribution of the strain tensor (eqs. 2–4) are assumed as follows:

$$\begin{aligned} \varepsilon_{11}^{0k} &= \alpha_1 + \alpha_2 x_2 && (17)\\ \varepsilon_{22}^{0k} &= \beta_1 + \beta_2 x_1 && (18)\\ 2\varepsilon_{12}^{0k} &= \gamma_1, && (19) \end{aligned}$$

while the *in-plane* flexural contribution are chosen to be:

$$\begin{aligned} \tilde{\varepsilon}_{11}^{k} &= \alpha_3 + \alpha_4 x_1 + \alpha_5 x_2 && (20)\\ \tilde{\varepsilon}_{22}^{k} &= \beta_3 + \beta_4 x_1 + \beta_5 x_2 && (21)\\ 2\tilde{\varepsilon}_{12}^{k} &= \gamma_2 + \gamma_3 (x_1)^2 + \gamma_4 (x_2)^2. && (22) \end{aligned}$$

The other strain components are evaluated with the procedure shown in eqs.(8)–(10); it should be noticed that, regardless of the number of layers, the strain field depends only on 14 independent parameters.

The displacement field can be conveniently expressed in terms of the in-plane displacements $\tilde{u}_1^{\ell}$, $\tilde{u}_2^{\ell}$ ($\ell = 1, \ldots, 4$), of the transverse displacements $\tilde{u}_3^{\ell}$ and of the rotations $\tilde{\varphi}_1^{\ell}$, $\tilde{\varphi}_2^{\ell}$ of transverse line elements, evaluated at the four nodes of the plate.

The components of the assumed displacement field are then functions of these nodal dofs and are expressed in terms of the usual Lagrangian shape functions as follows:

$$\begin{aligned} u_1 &= \sum_{\ell=1}^{4} N^{\ell}(\xi_i)\tilde{u}_1^{\ell} - x_3 \sum_{\ell=1}^{4} N^{\ell}(\xi_i)\tilde{\varphi}_1^{\ell} && (23)\\ u_2 &= \sum_{\ell=1}^{4} N^{\ell}(\xi_i)\tilde{u}_2^{\ell} - x_3 \sum_{\ell=1}^{4} N^{\ell}(\xi_i)\tilde{\varphi}_2^{\ell} && (24)\\ u_3 &= \sum_{\ell=1}^{4} N^{\ell}(\xi_i)\tilde{u}_3^{\ell}. && (25) \end{aligned}$$

where

$$N^{\ell}(\xi_i) = \frac{1}{4}(1 + \xi_1 \xi_1^{\ell})(1 + \xi_2 \xi_2^{\ell}) \quad (\ell = 1, \ldots, 4). \tag{26}$$

is the standard bilinear shape function of the isoparametric mapping. The dimensionless coordinates (ξ_1, ξ_2), with $-1 \leq \xi_i \leq 1$ (i=1, 2) are then related to the physical one x_1 and x_2 as follows:

$$x_i(\xi_i) = \sum_{\ell=1}^{4} N^{\ell}(\xi_i) x_i^{\ell} \tag{27}$$

where x_i^{ℓ}, (with $\ell = 1, \ldots, 4$), are the nodal coordinates of the element.

For the sake of conciseness the governing matrices, whose deduction follows the same procedure used for mixed-hybrid finite elements (see, for instance, [5]) are here skipped; it should be noticed, however that the presence of the the second-order work contribution $\frac{1}{2}\int_{\bar{\Omega}^e}\int_{h_{k-1}}^{h_k} \sigma_{ij}^{0k} u_{l,i} u_{l,j} \mathrm{d}x_3 \mathrm{d}A$ produces the usually denoted *geometric* stiffness matrix.

3 NUMERICAL RESULTS

The finite element described above has been used to evaluate the elastic buckling load of some homogeneous and laminated plates.

As a first step, some 1-D problems have been investigated. For them, the plate element described above reduces to a corresponding beam element: the relevant details are skipped for the sake of conciseness.

Subsequently, the plate problem has been tested on some truly 2-D problems.

3.1 *1-D buckling problems*

The buckling loads of both homogeneous and laminated beams have been computed by a usual eigenvalue analysis. Exact closed form solutions for homogeneous beams are easily available in the literature (see, e.g. [6] or [7]) for standard Bernoulli-Euler type beams (with no shear strain) and also for Timoshenko beams, where shear strain contribution is accounted for. Exact solutions for laminated beams are available only for some particular lamination sequences: see, for instance [1].

3.1.1 Homogeneous beams

As a first case, the buckling load of a cantilever beam has been computed for a thin beam (with a depth-to-span ratio $h/L = 0.02$) and for a thick one ($h/L = 0.25$). In both cases Poisson's ratio is $\nu = 0.3$ and cross-section is assumed to be square. For the *thin cantilever beam*, see Figure 3, the buckling load normalized against the exact value for an Euler-Bernoulli beam is shown in Table 1.

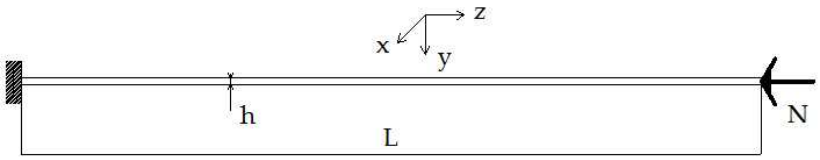

Figure 3: Thin cantilever beam.

# of el.	2-noded, Lagr.	3-noded, Lagr.	2-noded, Herm.
1	1.2158	1.0075	1.0075
2	1.0524	1.0005	1.0005
4	1.0129	1.0000	1.0000
8	1.0032	1.0000	1.0000
16	1.0008	1.0000	1.0000

Table 1: Normalized buckling load for a homogeneous cantilever beam $h/L = 0.02$

Here two- and three-noded elements with Lagrangian shape functions and two-noded elements with Hermitian shape functions have been tested: the last two cases produce the same result since for thin beams shear strain contribution is very small and the difference between section rotation and deformed axis slope is negligible. This means that constraining the axis slope is equivanlent (as it happens with Hermitian shape functions) to constraining the rotation of the cross section.

For the *thick cantilever beam*, Figure 4, the buckling load normalized against the exact value for a Timoshenko beam is shown in Table 2. In this case only Lagrangian shape functions have been

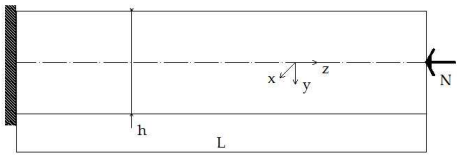

Figure 4: Thick cantilever beam.

# of el.	2-noded, Lagr.	3-noded, Lagr.
1	1.2058	1.0072
2	1.0503	1.0005
4	1.0124	1.0000
8	1.0031	1.0000
16	1.0008	1.0000

Table 2: Normalized buckling load for a homogeneous cantilever beam $h/L = 0.25$

considered, since, because of the appearence of shear strain, section rotation is different from the deformed axis slope, and the use of Hermitian shape function would not allow to enforce the exact boundary conditions. Before proceeding, it should be emphasized that minimal elements (i.e. elements with the fewest number of degrees-of- freedom (dofs) necessary to guarantee the absence of zero energy modes) do not behave optimally, in general, when the eigenvalue problem at hand is considered. Here the quadratic term in functional (15) corresponding to second-order work requires elements reacher than minimal ones to produce accurate results. That's why 3-noded elements performance is so far better.

3.1.2 Laminated beams

The buckling load of different kind of laminated cantilever beams has been computed. Mechanical data of the *laminae* are as follows:

$$\frac{E_1}{E_2} = 25; \quad G_{12} = G_{13} = 0.5E_2; \quad G_{23} = 0.2E_2; \quad \nu_{12} = 0.25$$

For the thin beam case, Figure 3, a depth-to-span ratio $h/L = 0.01$ was used. The buckling load is normalized against the exact value given in [1], p. 186, Table 4.2.4 and p. 200, Table 4.3.3; four different lamination sequences are considered (namely 0, 90, $(0/90)_s$, $(90/0)_s$) and the results are shown in Table 3. Here only two- and three-noded elements with Lagrangian shape functions have been considered.
For the thick beam case, Figure 4, a depth-to-span ratio $h/L = 0.05$ was used and the same 2- and 3-noded elements with Lagrangian shape functions were adopted. Results — only for lamination schemes 0, 90, $(0/90)_s$ — are shown in Table 4.

Lamin.	0	90	$(0/90)_s$	$(90/0)_s$	0	90	$(0/90)_s$	$(90/0)_s$
# of el.	(2-noded)				(3-noded)			
1	1.0511	1.0511	1.0139	1.0131	1.0075	1.0076	1.0068	1.0060
2	1.0010	1.0010	0.9998	0.9990	1.0005	1.0005	0.9998	0.9990
4	1.0001	1.0001	0.9988	0.9982	1.0000	1.0000	0.9993	0.9985
8	1.0000	1.0000	0.9987	0.9981	1.0000	1.0000	0.9993	0.9985
16	1.0000	1.0000	0.9987	0.9981	1.0000	1.0000	0.9993	0.9985

Table 3: Normalized buckling load for a laminated cantilever beam, $h/L = 0.01$

Lamin.	0	90	$(0/90)_s$	0	90	$(0/90)_s$
# of el.	(2-noded)			(3-noded)		
1	1.0126	1.0161	1.0313	1.0072	1.0073	1.0118
2	1.0035	1.0020	1.0147	1.0004	1.0003	1.0048
4	1.0024	1.0010	1.0126	1.0000	0.9999	1.0043
8	1.0022	1.0005	1.0123	1.0000	0.9999	1.0043
16	1.0021	1.0003	1.0122	1.0000	0.9999	1.0042

Table 4: Normalized buckling load for a laminated cantilever beam, $h/L = 0.05$

3.1.3 Homogeneous plates

Exact buckling loads of simply-supported, homogeneous thin plates under uniaxial compressive stresses or under shear stresses, as shown in Figure 5, are available in [7], p. 257–259 and p. 263–264, respectively.

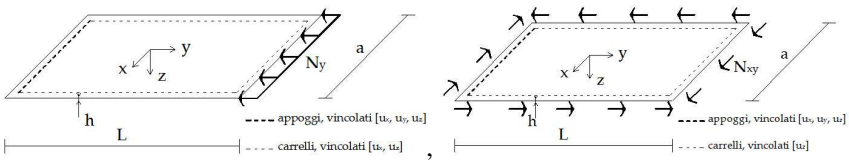

Figure 5: Simply-supported thin homogeneous plate under uniaxial compressive stresses and under shear stresses.

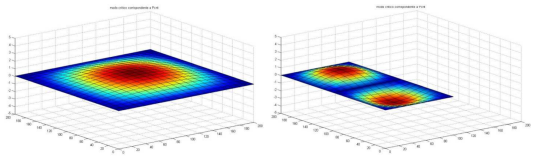

Figure 6: Critical modes for one square and for one rectangular thin homogeneous plate under compressive stresses.

	square plate (CS)			rectangular plate (CS)			square plate (SS)	
Mesh	Current	Straus7	Mesh	Current FE	Straus7	Mesh	Current	Straus7
2×2	1.0052	0.5520	1×2	—	0.2521	2×2	—	0.3468
4×4	0.9630	0.7032	2×4	0.9976	0.5603	4×4	1.3326	0.7779
8×8	0.9712	0.7516	4×8	0.9580	0.7040	8×8	1.0335	0.9347
20×20	0.9783	0.7663	10×20	0.9603	0.7575	20×20	0.9823	0.9873

Table 5: Normalized buckling load, under compressive stresses (CS) and under shear stresses (SS), for simply-supported plates, $h/L = 0.025$.

Data are as follows: Poisson's ratio $\nu = 0.3$, $h/L = 0.025$, $a/L = 1.$ (square plate) or $a/L = 2.$ (rectangular plate). Results in normalized form are compared in Table 5 with those provided by a commercial code (Straus7 version 2.3.6, developed and distributed by Strand7 Pty Ltd). The corresponding critical modes are shown in Figure 6 and 7.

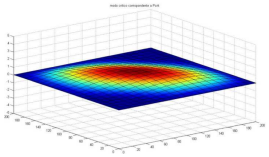

Figure 7: Critical modes for one square thin homogeneous plate under shear stresses.

As a last case, a relatively thick $h/L = 0.10$ simply-supported square plate under uniaxial compressive stresses (see Fig 5) is considered. Data are as in the previous case. The current solution, normalized by $D\pi/a^2$ — here $D = (1/12)Eh^3/(1-\nu^2)$ is the plate stiffness — is given in Table 6; for comparison purposes these results available in the literature are reported: Brunelle and Robertson [8] give 3.729; Reddy and Phan [9] 3.787; Doong [10] 3.730; Matsunaga [11] 3.771; in most cases these results are obtained by higher-order shear deformation theories.

Mesh	Current
2×2	4.9415
4×4	3.9300
8×8	3.7625
10×10	3.7324

Table 6: Normalized buckling load, under compressive stresses, for square simply-supported moderately thick plates, $h/L = 0.10$.

4 CONCLUSIONS

From the presented examples it appears that the proposed model allows to evaluate accurately the influence of shear deformations on critical loads: such an effect is expected to be significant in typical technical applications of composite laminated plates. Computationally speaking, its performances are fair, both in terms of efficiency and accuracy, when compared with other elements proposed in

the technical literature and/or implemented in available commercial finite element codes.

References

[1] Reddy, J. N. *Mechanics of laminated composite plates and shells - Theory and analysis*, CRC Press, Boca Raton (2004[2]).

[2] Cazzani, A., Garusi, E., Tralli, A., Atluri, S.N. "A four-node hybrid assumed strain finite element for laminated composite plates", *CMC: Computers, Materials & Continua*, **2**, 101–116, (2005).

[3] Cazzani, A., Battaglia, R., Benvenuti, E., Tralli, A. "A mixed plate model allowing for arbitrary delamination" in *Proc. ICCES'07*, Miami, FL, USA, January 3–8, 2007.(ISBN-13: 978-0-9717880-3-9).

[4] Washizu, K. *Variational methods in elasticity and plasticity*, Pergamon Press, Oxford (1982[3]).

[5] Pian, T.H.H., Wu, C.-C., *Hybrid and incompatible finite element methods*, Chapman & Hall/CRC, Boca Raton (2006).

[6] Timoshenko, S.P., Woinowsky-Krieger S. *Theory if plates and shells*, McGraw-Hill, New York (1959[2]).

[7] Corradi dell'Acqua L. *Meccanica delle strutture - vol. 3: la valutazione della capacità portante*, McGraw-Hill, Milano (1994).

[8] Brunelle, E.J., Robertson, S.R."Vibrations of an initially stressed thick plate", *J. Sound Vibr.*, **45**, 405–416,(1976).

[9] Reddy, J.N., Phan, N.D. "Stability and vibration of isotropic, orthotropic and laminated plates according to a higher-order shear deformation theory", *J. Sound Vibr.*, **98**, 157–170, (1985).

[10] Doong, J.-L. "Vibration and stability of an initially stressed thick plate according to a high-order deformation theory", *J. Sound Vibr.*, **113**, 425–440, (1987).

[11] Matsunaga, H. "Free vibration and stability of thick elastic plates subjected to in-plane forces", *Int. J. Solids Structures*, **31**, 3113–3124, (1994).